

# Learning complex models with invertible neural networks: a likelihood-free Bayesian approach

Stefan T. Radev<sup>1</sup>, Ulf K. Mertens<sup>1</sup>, Andreas Voss<sup>1</sup>, Lynton Ardizzone<sup>2</sup>, and Ullrich Köthe<sup>2</sup>

<sup>1</sup>Institute of Psychology, Heidelberg University, Hauptstr. 47-51, 69117 Heidelberg, Germany; <sup>2</sup>Heidelberg Collaboratory for Image Processing (HCI), Interdisciplinary Center for Scientific Computing (IWR), Heidelberg University, Im Neuenheimer Feld 205, 69120 Heidelberg, Germany

This manuscript was compiled on June 28, 2019

1 Parametric models of complex processes are ubiquitous throughout the sciences. As the processes under study and the models describing  
2 them become increasingly complex, parameter estimation with standard Bayesian and frequentist methods can quickly become intractable.  
3 To address this, we propose a novel method for likelihood-free inference based on invertible neural networks. The method is capable of  
4 performing fast full Bayesian inference on large amounts of data by training the networks on simulated data and learning to invert the model  
5 under study. The method is independent of particular data formats, as it includes a summary network trained to embed the observed data  
6 into fixed-size vectors in a data-driven way. This makes the method applicable to various scenarios where standard inference techniques fail.  
7 We demonstrate the utility of the method on a toy model with known analytic posterior and on example models from population dynamics,  
8 epidemiology, cognitive science and genetics. We argue for a general framework for building reusable parameter estimation machines for  
9 potentially any process model from which simulations can be obtained.

Deep learning | Invertible networks | Bayesian inference | Parameter estimation | Stochastic models

**M**athematical models are formal descriptions of scientific theories allowing a clear and unambiguous way to formulate and test scientific hypotheses about probabilistic phenomena in a probabilistic world. In its most abstract form, a mathematical model is specified by a set of parameters  $\theta$  and a forward model  $q$  mimicking the process by which manifest data  $x$  arise from latent parameters:

$$x = q(\theta) \quad [1]$$

1 While  $q$  can represent an arbitrarily complex process by an arbitrarily complicated expression, its functional form is usually  
2 guided by a well-founded theoretical framework. For instance,  $q$  can be a stochastic differential equation describing the dynamics  
3 of single neurons in the brain, or a step-by-step biological algorithm dictating the rate of gene expression in certain cells. Thus,  
4 it is only through theoretical embedding that a meaningful interpretation in terms of some mechanism can be attached to  
5 the parameters of a mathematical model. Examples of mathematical models can be found in various scientific domains, e.g.,  
6 genetics (1, 2), cognitive science (3, 4), neuroscience (5, 6), population dynamics (7), epidemiology (8, 9), just to name a few.

7 Once a mathematical model has been formulated, the next step consists of fitting the model to experimental or observational  
8 data and recovering the parameters of interest. However, estimating the parameters of a mathematical model from data  
9 can quickly become one of the most tenacious challenges in applications to real-world problems. It is also one of the most  
10 important ones to be tackled, since without reliable parameter estimation methods, it is impossible to test the utility of a  
11 model, regardless of its sophistication or theoretical appeal. Idealized parameter estimation involves computing the inverse  
12 (backward) model  $\theta = q^{-1}(x)$  exactly. However, due to noise, inherent stochasticity or loss of information, the inverse usually  
13 does not exist, so researchers need to resort to the sophisticated frameworks of Bayesian or frequentist inference.

14 However, as mathematical models and processes under description become increasingly complex, parameter estimation and  
15 model selection can quickly become intractable with standard Bayesian and frequentist method. Complex models specified by  
16 a generative stochastic mechanism do not always provide a closed-form solution for the *likelihood function* (3, 10, 11). This  
17 poses great difficulties for Bayesian and frequentist methods alike, since both depend explicitly on the numerical evaluation  
18 of a likelihood function as a proxy for assessing model fit to data. Even if a likelihood function is available in closed-form,

## Significance Statement

Describing complex stochastic processes with parametric models lies at the heart of science. Simulating models given a set of parameters is relatively easy with the aid of modern computers, but inferring model parameters from observed data can often be a challenging endeavor. We combine recent advances in deep learning and Bayesian inference into a powerful method for building reusable parameter estimation networks applicable to various types of models and data encountered in different research fields.

Please provide details of author contributions here.

This research was supported by the Deutsche Forschungsgemeinschaft (DFG, German Research Foundation; grant number GRK 2277 "Statistical Modeling in Psychology")

<sup>2</sup>To whom correspondence should be addressed. E-mail: stefan.ralev@psychologie.uni-heidelberg.de

19 inference may be prohibitively slow for real-world applications. In this case, enforcing simplifying distributional assumptions  
20 (i.e., independence or Gaussian assumptions) on the likelihood can increase the speed of inference, but can also lead to model  
21 misspecifications and dramatically incorrect estimates. Therefore, the need for powerful and reliable likelihood-free estimation  
22 methods arises naturally.

23 Likelihood-free methods aim at bypassing the above problems by resorting to a simulation-based approach to parameter  
24 estimation and model selection (3, 12). A subset of likelihood-free methods includes approximate Bayesian computation (ABC)  
25 methods, which aim at preserving the advantages of Bayesian data analysis even when the likelihood function is intractable or  
26 practically impossible to compute (10, 12, 13). ABC methods approximate the likelihood function by repeatedly sampling  
27 parameters from a pre-specified prior distribution  $p(\boldsymbol{\theta})$  and then simulating multiple datasets by running the generative model  
28  $q(\boldsymbol{\theta})$  using the sampled parameters. Thus, the core ingredients of ABC methods are a prior on  $\boldsymbol{\theta}$ , and a generative model  $q(\boldsymbol{\theta})$ ,  
29 usually specified as a function code in a general-purpose programming language (10, 14).

30 Performing approximate inference comes at the cost of incurring additional approximation error, which accumulates on  
31 top of the irreducible estimation error. Within the context of approximate inference, the most common manifestations of  
32 approximation error include: *i*) imprecise form of the posterior; *ii*) imprecise posterior moments; *iii*) under- or overestimation  
33 of uncertainty. Different approximation methods usually involve multiple trade-offs between minimizing approximation error  
34 and keeping computational time within reasonable bounds (3, 15).

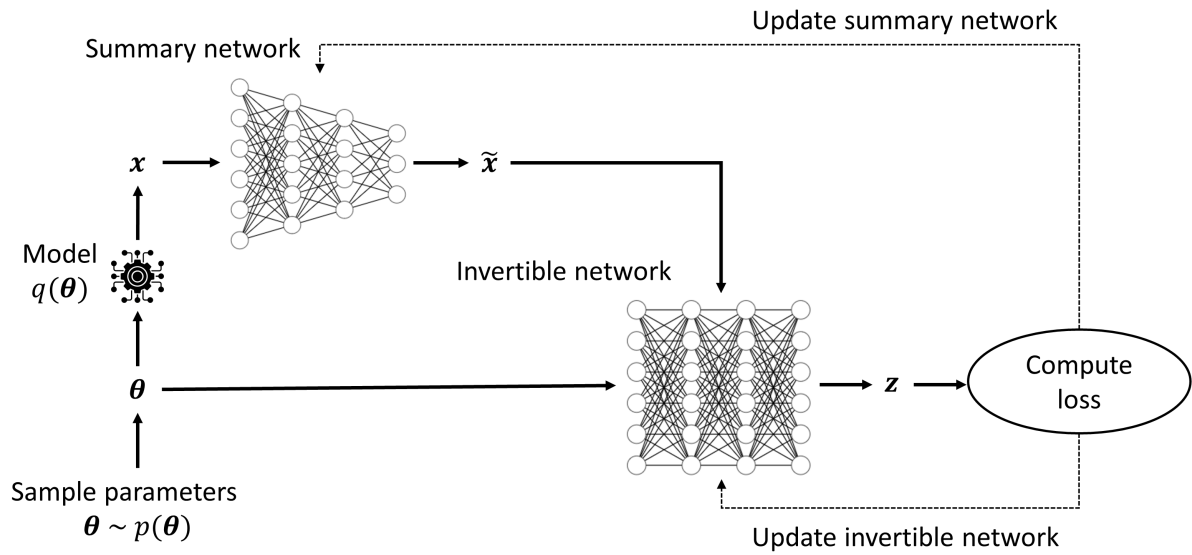
35 Recently, ideas from machine learning and deep learning research have entered the field of likelihood-free inference in  
36 an attempt to overcome some of the shortcomings of traditional methods (5, 6, 16–20). The most common approach has  
37 been to cast the problem of parameter estimation as a supervised learning task. In this setting, a large dataset of the form  
38  $\mathcal{D} = \{h(\mathbf{x}^{(i)}), \boldsymbol{\theta}^{(i)}\}_{i=1}^n$  is created by repeatedly sampling from  $p(\boldsymbol{\theta})$  and simulating an artificial dataset  $\mathbf{x}$  by running  $q(\boldsymbol{\theta})$  with  
39 the sampled parameters. Usually, the dimensionality of the simulated data is reduced by computing summary statistics with  
40 a fixed summary function  $h(\mathbf{x})$ . Then, a supervised learning algorithm  $f(h(\mathbf{x}); \boldsymbol{\phi}) = \hat{\boldsymbol{\theta}}$  with learnable parameters  $\boldsymbol{\phi}$  (e.g.,  
41 linear regression, random forest, neural network) is trained on the simulated data to later output an estimate of the true data  
42 generating parameters. Thus,  $f(h(\mathbf{x}); \boldsymbol{\phi})$  essentially attempts to “learn” the intractable inverse model  $\boldsymbol{\theta} = q^{-1}(\mathbf{x})$ .

43 Inspired by previous machine learning approaches, the current work proposes a novel and universal likelihood-free method  
44 capable of performing full Bayesian inference on any mathematical process model from which simulations can be obtained. It  
45 treats parameter inference as a task of inverting a generative model and achieves this by drawing on the modern framework  
46 of deep probabilistic modeling for tackling intractable posteriors (21–24). The method integrates two separate deep neural  
47 networks modules (detailed in the **Methods** section; see Figure 1) trained jointly on simulated data: a *summary network* and  
48 an *invertible network*.

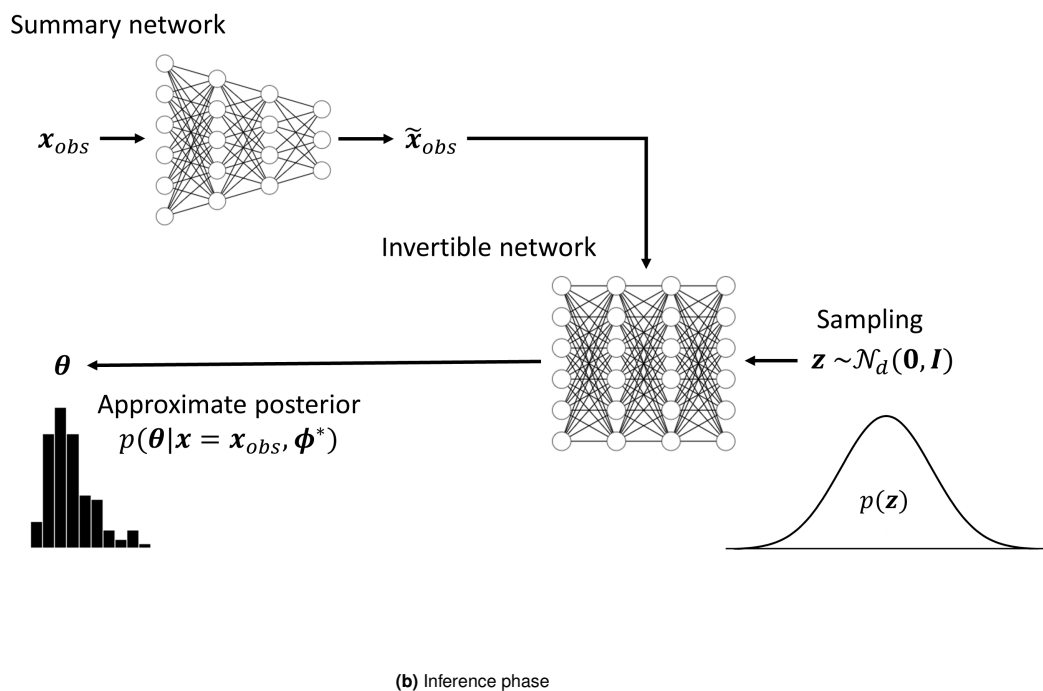
49 The *summary network* is responsible for learning the most informative summary statistics directly from data. It should be  
50 designed to follow the functional and probabilistic symmetries inherent in the data, e.g. a permutationally invariant network for  
51 *i.i.d.* data (25), a recurrent network for time-series data, or a convolutional network for grid-like data (26). The computation  
52 of summary statistics is a crucial aspect in likelihood-free inference. Previous approaches mainly use hand-crafted summary  
53 statistics tailored to the specific application. However, in many application, it is not straightforward to settle upon a set of  
54 good summary statistics. Thus, the summary network completely eliminates the need to manually specify a fixed number of  
55 summary statistics and makes the method independent of the format or the size of the data.

56 The *invertible network* is responsible for learning the posterior of the model parameters given the observed and summarized  
57 data. It is based on the recently developed flow-based architecture (22–24). Flow-based methods provide exact latent-variable  
58 inference and log-likelihood evaluation when operating at optimum. In the **Methods** section, we show that our method  
59 maximizes the posterior over model parameters directly when cast in the context of likelihood-free inference. Furthermore,  
60 flow-based methods are capable of approximating very high-dimensional distributions (e.g., the pixels of an image). Once  
61 trained with a sufficient amount of simulated data, our invertible network can perform full Bayesian inference on large amounts  
62 of real data from a given domain in a single pass. The joint training of a summary network and an invertible network results  
63 in a powerful and universal parameter estimation machine capable of inverting complicated statistical problems in various  
64 scientific domains (Figure 1). Moreover, the method addresses many of the limitations of previous likelihood-free methods.  
65 First, it involves no costly MCMC or rejection sampling, which makes the inference phase lightning fast, as we also make use of  
66 GPU-accelerated computation. Second, it involves no fixed summary statistics or kernels, but learns the most informative  
67 representation of the data in an end-to-end manner. Third, the method is fully Bayesian, as it directly learns the posterior over  
68 model parameters and thus allows for the quantification of uncertainty, which is a crucial requirement in parameter estimation  
69 (27, 28). Last, the trained networks can be shared and reused by multiple researches within a scientific domain, thus removing  
70 the need for wasteful computations and fitting a separate model for each and every dataset. This pooling of computational  
71 resources across researches is an important step forward in mathematical modeling, as has been recently argued (17).

72 To illustrate the utility of the new method, we first apply it to a toy Bayesian regression model with known posterior. Then,  
73 we present applications to intractable models from cognitive science, population dynamics, epidemiology, and genetics and  
74 demonstrate state-of-the art parameter recovery. Across the examples, we introduce multiple tools to validate the performance  
75 of our method. The outline of the remaining manuscript is as follows: The **Methods** section introduces the main building  
76 blocks of the new method and summarizes the main steps as pseudocode. The **Results** section presents the various applications  
77 of the model to real-world research domains. Finally, the **Discussion** section lists the advantages of the current method, treats  
78 some potential pitfalls and explores future research vistas. Python code and simulation scripts for all current applications are  
79 freely available as Jupyter notebooks at <https://github.com/stefanradev93/cINN> and as a small library based on *TensorFlow*



(a) Training phase



(b) Inference phase

**Fig. 1.** Graphical illustration of the method. **(a)** During the training phase, the summary and the invertible network are trained on simulated data from the model and updated after each batch of simulations; **(b)** During the inference phase, the true posterior of the model parameters is approximated from real data using the trained networks. Thus, knowledge about the relationship between parameters and data (the mathematical model) is compactly encoded within the weights of the two networks. The trained networks can then be shared and used across researchers working on the same model.

80 (29) for creating and training custom invertible networks with GPU support, along with some validation tools.

## 81 Methods

82 **Notation.** In the following, we denote observed or simulated univariate datasets from the mathematical model of interest as  
83  $\mathbf{x} = (x_1, x_2, \dots, x_n)$ , and multivariate datasets as  $\mathbf{X} = (\mathbf{x}_1, \mathbf{x}_2, \dots, \mathbf{x}_n)$ . The parameters of a mathematical model are represented  
84 as a vector  $\boldsymbol{\theta} = (\theta_1, \theta_2, \dots, \theta_d)$ , and all trainable parameters of the invertible and summary neural networks as  $\phi = (\phi_{inv}, \phi_{sum})$ .  
85 The number of parameters of a mathematical model will be denoted as  $d$ , and the number of simulated data points as  $n$ .

86 **Deep Probabilistic Modeling.** Our method draws on major advances in modern deep probabilistic modeling, also referred to  
87 as deep generative modeling (21, 22, 25, 30). A hallmark idea in deep probabilistic modeling is to handle intractable target  
88 probability distributions by sampling from simpler distributions (e.g., Gaussian or uniform distributions) and transforming these  
89 samples via a complex non-linear, learnable transformations. Most popular deep probabilistic models entail two phases. During  
90 the *training phase*, a transformation from the simple to the desired target distribution is learned by optimizing a cost function  
91 via backpropagation (see Figure 1a). During the *inference phase*, samples from the target distribution are obtained by sampling  
92 from the simple distribution and applying the transformation learned during the training phase (see Figure 1b). Using this  
93 approach, recent applications of deep probabilistic models have achieved unprecedented results on extremely high-dimensional  
94 and intractable problems (e.g., complex data distributions such as natural images, music, or text).

95 In the context of mathematical modeling and Bayesian inference, the target distribution is the posterior distribution of model  
96 parameters  $p(\boldsymbol{\theta}|\mathbf{x})$  capturing our uncertainty about the numerical values of parameters given empirical data. We can leverage  
97 the fact that most mathematical models are generative in nature and as such can be used to perform multiple simulations  
98 of the process of interest. By specifying a prior distribution over the model parameters  $p(\boldsymbol{\theta})$ , one can generate arbitrarily  
99 large datasets of the form  $\mathbf{D} = \{\mathbf{x}^{(i)}, \boldsymbol{\theta}^{(i)}\}_{i=1}^n$  and use a deep generative model to learn a probabilistic mapping from data  
100 to parameters. Thus, at inference time, one can condition the model on observed data  $\mathbf{x}_{obs}$  and obtain samples  $\boldsymbol{\theta}_1, \boldsymbol{\theta}_2, \dots, \boldsymbol{\theta}_L$   
101 approximating the posterior  $p(\boldsymbol{\theta}|\mathbf{x} = \mathbf{x}_{obs})$  in the manner described above.

102 In the current work, we propose to implement and use a conditional invertible neural network (cINN) architecture. Previously,  
103 INNs have been successfully employed to model data from astrophysics and medicine (21). We adapt the model to suit the task  
104 of parameter estimation in the context of mathematical modeling (see Figure 1 for a full graphical illustration of the method)  
105 and develop a reusable probabilistic architecture for full Bayesian likelihood-free inference on complex mathematical models.

**The Affine Coupling Block.** The basic building block of a cINN is the affine coupling block (ACB, see Figure 2a) (21, 22, 24).  
Each cACB consists of four separate fully connected neural networks denoted as  $s_1(\cdot), s_2(\cdot), t_1(\cdot), t_2(\cdot)$ . An ACB is specifically  
designed to be invertible, which means that in addition to a parametric mapping  $f_{\phi_{inv}} : \mathbb{R}^d \rightarrow \mathbb{R}^d$  it also learns the inverse  
mapping  $f_{\phi_{inv}}^{-1} : \mathbb{R}^d \rightarrow \mathbb{R}^d$  "for free". Denoting the input vector of  $f_{\phi_{inv}}$  as  $\mathbf{u}$  and the output vector as  $\mathbf{v}$ , it follows that  
 $f(\mathbf{u}; \phi_{inv}) = \mathbf{v}$  and  $f^{-1}(\mathbf{v}; \phi_{inv}) = \mathbf{u}$ . Invertibility is achieved by splitting the input vector into two parts  $\mathbf{u} = (\mathbf{u}_1, \mathbf{u}_2)$  and  
performing the following operations on the split input:

$$v_1 = u_1 \odot \exp(s_1(u_2)) + t_1(u_2) \quad [2]$$

$$v_2 = u_2 \odot \exp(s_2(v_1)) + t_2(v_1) \quad [3]$$

The outputs  $\mathbf{v} = (v_1, v_2)$  are then concatenated again and passed to the next ACB. The inverse operation is given by:

$$u_2 = (v_2 - t_2(v_1)) \odot \exp(-s_2(v_1)) \quad [4]$$

$$u_1 = (v_1 - t_1(u_2)) \odot \exp(-s_1(u_2)) \quad [5]$$

106 An additional property of this design, which becomes relevant later for optimization, is that the operations of the ACB have  
107 tractable, and cheaply computable Jacobians (strictly upper or lower triangular matrices). Furthermore, the internal networks  
108  $s_1(\cdot), s_2(\cdot), t_1(\cdot), t_2(\cdot)$  can be represented by arbitrarily complex neural networks, which themselves need not be invertible, since  
109 they are only ever evaluated in the forward direction during both the forward and the inverse pass through the ACB. To ensure  
110 that the model is powerful enough to represent complicated distributions, we chain multiple ACBs, so that the output of each  
111 ACB becomes the input of the next (see Figure 2b). In this way, the whole chain remains invertible from the first input to the  
112 last output and can be viewed as a single function parameterized by trainable parameters  $\phi_{inv}$ .

In our applications, the input to the first ACB is the parameter vector  $\boldsymbol{\theta}$ , and the output of the final ACB, denoted  
hitherto as  $\mathbf{z}$ , is encouraged to follow a  $d$ -dimensional spherical Gaussian via optimization (described in detail later), that is,  
 $p(\mathbf{z}) = \mathcal{N}_d(\mathbf{z}|\mathbf{0}, \mathbf{I})$ . Fixed permutation matrices are used before each ACB to ensure that each axis of the latent space encodes  
information from all components of  $\boldsymbol{\theta}$ . In order to take into account the observed data  $\mathbf{x}$ , each of the internal networks of each  
ACB is augmented to take  $\mathbf{x}$  as an additional input -  $s_1(\cdot, \mathbf{x}), s_2(\cdot, \mathbf{x}), t_1(\cdot, \mathbf{x}), t_2(\cdot, \mathbf{x})$  - so a complete pass through the entire  
invertible chain can be expressed as:

$$f(\boldsymbol{\theta}; \mathbf{x}, \phi_{inv}) = \mathbf{z} \quad [6]$$

together with the inverse operation:

$$f^{-1}(\mathbf{z}; \mathbf{x}, \phi_{inv}) = \boldsymbol{\theta} \quad [7]$$

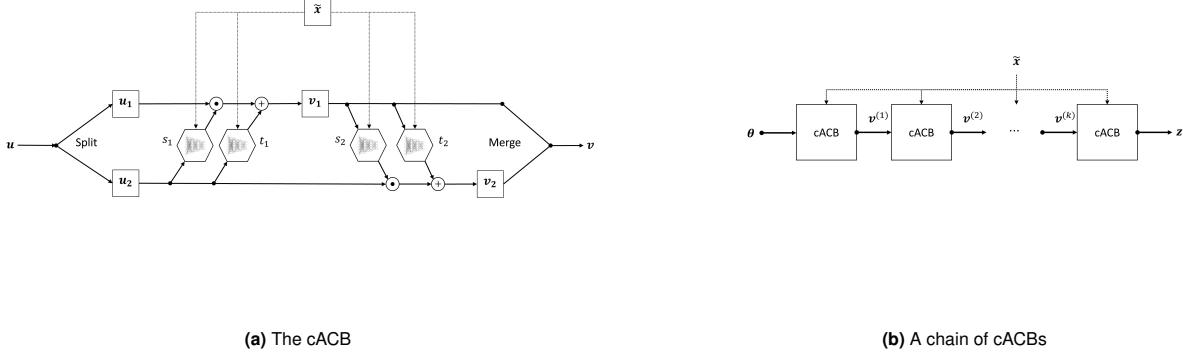


**Fig. 2.** A diagram of the conditional version of the affine coupling block (cACB). **(a)** Each cACB consists of four internal networks performing the invertible operations described in the text; **(b)** In practice, we chain multiple cACBs to obtain higher representational capacity. Each cACB layer uses a fixed permutation to ensure that information about each parameter is encoded in each latent dimension of  $\mathbf{z}$ .

This process can be interpreted as follows: the forward pass maps data-generating parameters to  $\mathbf{z}$ -space using conditional information of  $\mathbf{x}$ , while the inverse pass maps data points from  $\mathbf{z}$ -space to the data-generating parameters of interest using the same conditional information provided by the data. In the next section, we describe the optimization procedure used to match the outputs of  $f^{-1}(\mathbf{z}; \mathbf{x}, \phi_{inv})$  to the posterior  $p(\theta|\mathbf{x})$ .

**Summary Network.** Since in practice the conditioning data set  $\mathbf{x}$  can have variable number of input points (e.g., trial sizes, time points) and exhibit various redundancies, the cINN can profit from some form of dimensionality reduction applied to the data. Ideally, we want to avoid hand-crafted summary statistics, and instead learn the most informative summary statistics directly from data. Therefore, instead of feeding the raw simulated (observed) data to each ACB, we pass the data through an additional summary network to obtain a fixed-sized vector of learned summary statistics  $\tilde{\mathbf{x}} = h(\mathbf{x}; \phi_{sum})$  and learn the parameters of the summary network  $h$  jointly with those of the cINN chain via backpropagation. Thus, the current method remains completely end-to-end and is capable of generalizing to data sets of variable input size and structure.

**Learning the Posterior.** The cINN learns to approximate the posterior of model parameters by optimizing a maximum likelihood (ML) criterion. Broadly speaking, the goal of ML estimation is to find a set of parameters which maximize the probability of the data under a parametric model. In our case, we are interested in maximizing the expectation over all possible neural network parameters with respect to the parameters of the mathematical model:

$$\phi^* = \underset{\phi}{\operatorname{argmax}} \mathbb{E}_{\theta \sim p(\theta|\mathbf{x})} [p(\phi|\theta, \mathbf{x})] \quad [8]$$

Applying Bayes' rule to the posterior over all neural network parameters we obtain:

$$p(\phi|\theta, \mathbf{x}) \propto p(\theta|\mathbf{x}, \phi)p(\phi) \quad [9]$$

Note, that by maximizing Eq. 9 we are maximizing the posterior over model parameters of interest  $p(\theta|\mathbf{x}, \phi)$ . Thus, it remains to find a tractable expression for Eq. 8 to be minimized by backpropagation given a finite number of simulated samples from the model. To this end, we recall that we can relate the pdf of  $\theta$  to that of  $\mathbf{z}$  via the change of variable theorem:

$$p(\theta|\mathbf{x}, \phi) = p(\mathbf{z}) \left| \det \left( \frac{\partial \mathbf{z}}{\partial \theta} \right) \right| \quad [10]$$

$$= p(f(\theta; \mathbf{x}, \phi)) \left| \det \left( \frac{\partial f}{\partial \theta} \right) \right| \quad [11]$$

where  $\partial f / \partial \theta = \mathbf{J}_f$  is the Jacobian of the learned transformation  $f(\theta; \mathbf{x}, \phi)$  with respect to the input. Both terms in Eq. 11 are now tractable, since we have previously defined  $\mathbf{z}$  as following a spherical unit Gaussian, that is,  $p(\mathbf{z}) = (2\pi)^{-d/2} \exp(-\|\mathbf{z}\|_2^2)$  and the log determinant of the Jacobian is easily computed as  $s_1(\mathbf{u}_2, \mathbf{x}) + s_2(\mathbf{v}_1, \mathbf{x})$  due to eqs. 2 and 3. We can now formulate the ML loss as the Monte-Carlo approximation of the negative logarithm of Eq. 8 for a batch of size  $m$ :

$$\mathcal{L}(\phi) = -\frac{1}{m} \sum_{i=1}^m \log (p(\phi|\theta^{(i)}, \mathbf{x}^{(i)})) \quad [12]$$

$$= -\frac{1}{m} \sum_{i=1}^m \log (p(\theta^{(i)}|\mathbf{x}^{(i)}, \phi)p(\phi)) \quad [13]$$

$$= -\frac{1}{m} \sum_{i=1}^m \left( \frac{\|f(\theta^{(i)}; \mathbf{x}^{(i)}, \phi)\|_2^2}{2} + \log \left| \det \left( \mathbf{J}_f^{(i)} \right) \right| \right) + \tau \|\phi\|_2^2 \quad [14]$$

124 where we place a Gaussian prior over the neural network parameters with  $\tau \equiv 1/\sigma^2$ , corresponding to a standard L2-  
 125 regularization.

126 Minimizing Eq. 14 can be interpreted as searching for the optimal neural network parameters  $\phi^*$  which maximize the  
 127 probability of model parameters  $\theta$  given data  $x$ . This is exactly the probability we are concerned with in Bayesian inference.  
 128 Note that our formulation maximizes the posterior of model parameters directly, in contrast to variational methods which  
 129 optimize a lower bound on the posterior (20, 30). Once the backpropagation algorithm has settled to a local minimum of the ML  
 130 loss, one can easily obtain samples from the approximate posterior  $p(\theta|x = x_{obs}, \phi = \phi^*)$ , based on an observed dataset  $x_{obs}$ , by  
 131 repeatedly sampling  $z^{(l)} \sim \mathcal{N}_d(\mathbf{0}, \mathbf{I})$ , and then passing  $z^{(l)}$  in reverse to the cINN in order to compute  $\theta^{(l)} = f^{-1}(z^{(l)}; x_{obs}, \phi^*)$   
 132 for  $l = 1, \dots, L$ . Figure 1b illustrates the inference phase of the method. It is worth noting that sampling a large number of  
 133 parameter values from the approximate posterior takes a negligible amount of time, since it only requires a single pass through  
 134 the cINN in reverse.

135 **Training the Networks.** We train all cINNs and summary networks described in this paper jointly via backpropagation. For all  
 136 following experiments, we use the Adam optimizer with a starter learning rate of  $10^{-3}$  and an exponential decay rate of .95.  
 137 We set the weight regularization parameter  $\tau$  to a value of  $10^{-5}$ . We perform 1000000 iterations (network updates) for each of  
 138 the examples in this paper, and report the results on the trained network. Note, that we did not perform an extensive search  
 139 for optimal values of the cINN hyperparameter but use a cINN with 10 ACBs for each example in this paper (see SI for details  
 140 of the cINN). Concerning the data generation step, we use two training approaches. The first follows the classical approximate  
 141 Bayesian computation approach to create a large “reference table” or grid of the form  $D = \{\mathbf{x}^{(i)}, \theta^{(i)}\}_{i=1}^n$ . The reference table  
 142 is then used as training data for the neural network and training continues for a pre-specified number of epochs through the  
 143 entire reference table. A separate validation dataset is eventually used to assess the performance of the network. This training  
 144 approach separates the simulation from the training phase but can incur large memory overhead, as the reference table must  
 145 be stored on disk and then loaded in chunks or in its entirety into memory. The second approach follows a different strategy,  
 146 which is used mainly in the field of active learning. Correspondingly, a dataset, or a batch of datasets, is created on the fly and  
 147 then passed through the neural network. This training regime has the advantage that the network never “experiences” the  
 148 same input data twice. Moreover, training can continue as long as the network keeps improving (i.e., the loss keeps decreasing),  
 149 since overfitting in the classical sense is nearly impossible. However, if the simulations are computationally expensive and  
 150 researchers need to experiment with multiple models, it might be beneficial to switch to the first regime, since simulation and  
 151 training in the active learning regime are tightly intertwined. TODO - Describe for which!

152 **Putting It All Together.** On an abstract level, our method requires three key ingredients: 1) a mathematical process model  
 153  $q(\theta)$  capable of simulating data  $x$ ; 2) a prior distribution over the model parameters  $p(\theta)$  encoding our prior beliefs about  
 154 plausible parameter values; 3) an invertible neural network  $f_\phi$  capable of approximating a large enough family of probability  
 155 distributions (see Figure 2). In practice, a chain of up to 10 ACBs should suffice to learn most distributions encountered in the  
 156 life sciences, since they tend to be unimodal and relatively simple (in contrast to the distribution of natural images or words in  
 157 a spoken language). From these three ingredients, a universal and reusable sampler can be designed for likelihood-free Bayesian  
 158 estimation of both tractable and intractable mathematical models. **Algorithm 1** describes the essential steps of the method  
 159 using an arbitrary summary network and employing the active learning training regime.

---

#### Algorithm 1 Bayesian likelihood-free inference with invertible neural networks

---

- 1: *Training (via active learning):*
  - 2: **repeat**
  - 3:   Sample a batch of  $\{\theta^{(i)}\}_{i=1}^m$  from prior  $p(\theta)$
  - 4:   Simulate a batch of datasets  $\{\mathbf{x}^{(i)}\}_{i=1}^m$  by running  $\mathbf{x}^{(i)} = q(\theta^{(i)})$  for  $i = 1, \dots, m$
  - 5:   Pass  $\{\mathbf{x}^{(i)}\}_{i=1}^m$  through summary network  $h(\mathbf{x}^{(i)}; \phi_{sum})$  to obtain  $\{\tilde{\mathbf{x}}^{(i)}\}_{i=1}^m$
  - 6:   Pass  $\{\theta^{(i)}\}_{i=1}^m$  and  $\{\tilde{\mathbf{x}}^{(i)}\}_{i=1}^m$  through cINN  $f(\theta^{(i)}; \mathbf{x}^{(i)}, \phi_{inv})$  to obtain  $\{z^{(i)}\}_{i=1}^m$
  - 7:   Compute ML loss  $\mathcal{L}(\phi)$  according to Eq.14
  - 8:   Update neural network parameters  $\phi$  via backpropagation
  - 9: **until** convergence to  $\phi^*$
  - 10: *Inference (given observed or test data  $x_{obs}$ ):*
  - 11: Summarize the observed data by computing  $\tilde{\mathbf{x}}_{obs} = h(\mathbf{x}_{obs}, \phi_{sum}^*)$
  - 12: **for**  $l = 1, \dots, L$  **do**
  - 13:   Sample  $z^{(l)} \sim \mathcal{N}_d(\mathbf{0}, \mathbf{I})$
  - 14:   Compute  $\theta^{(l)} = f^{-1}(z^{(l)}; \tilde{\mathbf{x}}_{obs}, \phi_{inv})$
  - 15: **end for**
  - 16: Use  $\{\theta^{(l)}\}_{l=1}^L$  to approximate the posterior  $p(\theta|x_{obs})$
- 

160 The backpropagation algorithm works by computing the gradients of the loss function w.r.t. the parameters of the neural  
 161 networks and then adjusting the parameters, so as to drive the loss function to a local minimum. We experienced no instability  
 162 or convergence issues during training with the ML loss. Note, that steps 12 – 15 of **Algorithm 1** can be executed in parallel  
 163 with GPU support.

164 In what follows, we apply the method to a toy Bayesian regression example with conjugate priors, and then use it to estimate  
 165 the parameters of challenging models from population dynamics, cognitive science, epidemiology, and genetics. Code for  
 166 reproducing the results on all following examples is freely available at: <https://github.com/stefanradev93/cINN>. All examples  
 167 are implemented in Python using the *TensorFlow* library.

## 168 Results

169 We consider a number of metrics for determining the performance of our method. To assess the goodness of parameter  
 170 recovery, we compute the normalized root mean squared error (NRMSE) and the coefficient of determination ( $R^2$ ) metrics of  
 171 the parameter estimates. To assess the recovery of the full posterior, we compute the Kullback-Leibler (KL) divergence (31)  
 172 between the true and the approximate distributions for the toy example, and use simulation-based calibration (SBC, (32)) for  
 173 the other examples where the analytic posterior is not available in closed-form. Details for computing the *NRMSE*,  $R^2$ , and  
 174 SCB can be found in the **SI**.

**Toy Example – Bayesian Regression.** As a proof-of-concept, we demonstrate the utility of our method in recovering the true analytic posteriors of the regression coefficients of a conjugate Bayesian regression model. To set the setting, assume we have observed a dataset  $\mathbf{D} = \{\mathbf{x}^{(i)}, y^{(i)}\}_{i=1}^n$  with  $\mathbf{x} \in \mathbb{R}^d$  and  $y \in \mathbb{R}$ . We model each  $y^{(i)}$  as being conditionally Gaussian given  $x^{(i)}$ , i.e.,  $y^{(i)} \sim \mathcal{N}(\boldsymbol{\theta}^T \mathbf{x}^{(i)}, a^{-1})$  where  $\boldsymbol{\theta} \in \mathbb{R}^d$  and  $a$  is the precision (inverse noise variance,  $a \equiv 1/\sigma_y^2$ ). We place a  $d$ -dimensional diagonal Gaussian prior on the regression coefficients centered at 0:  $\boldsymbol{\theta} \sim \mathcal{N}_d(\mathbf{0}, b^{-1}\mathbf{I})$  where  $b$  is the precision of the prior ( $b \equiv 1/\sigma_\theta^2$ ). Thus, the likelihood  $p(\mathbf{D}|\boldsymbol{\theta})$  admits the following proportionality:

$$p(\mathbf{D}|\boldsymbol{\theta}) \propto \exp\left(-\frac{a}{2} (y - \mathbf{X}\boldsymbol{\theta})^T (y - \mathbf{X}\boldsymbol{\theta})\right) \quad [15]$$

where  $\mathbf{X}$  denotes the design matrix containing all  $\mathbf{x}^{(i)}$  stacked row-wise. Since the prior of  $\boldsymbol{\theta}$  is conjugate to the likelihood (both are Gaussian distributions), the posterior of  $\boldsymbol{\theta}$  is also Gaussian, given by:

$$p(\boldsymbol{\theta}|\mathbf{D}) \propto \exp\left(-\frac{a}{2} (y - \mathbf{X}\boldsymbol{\theta})^T (y - \mathbf{X}\boldsymbol{\theta}) - \frac{b}{2} \boldsymbol{\theta}^T \boldsymbol{\theta}\right) \quad [16]$$

Therefore, the posterior has the form  $p(\boldsymbol{\theta}|\mathbf{D}) = \mathcal{N}_d(\boldsymbol{\theta}|\boldsymbol{\mu}, \boldsymbol{\Lambda}^{-1})$  where  $\boldsymbol{\Lambda}$  denotes the posterior precision matrix (inverse covariance matrix),  $\boldsymbol{\mu}$  the posterior mean vector, which are computed as follows:

$$\boldsymbol{\Lambda} = a\mathbf{X}^T \mathbf{X} + b\mathbf{I} \quad [17]$$

$$\boldsymbol{\mu} = a\boldsymbol{\Lambda}^{-1} \mathbf{X}^T \mathbf{y} \quad [18]$$

175 Thus, for known  $a$  and  $b$ , the posterior can be easily computed. Even though in real-world applications  $a$  is usually not known  
 176 and a hierarchical model is used instead, the current example is good for testing the utility of our method.

177 For the following application, we set  $d = 4$ , and  $a = b = 1$ . The design matrices for each iteration contain a variable number  
 178  $n$  of *i.i.d.* data points drawn from a unit Gaussian  $\mathbf{x}^{(i)} \sim \mathcal{N}_4(\mathbf{0}, \mathbf{I})$  for  $i = 1, \dots, n$ . The number of trials is drawn from a  
 179 uniform distribution  $n \sim \mathcal{U}(50, 500)$  at each training iteration (Lines 2-9 of **Algorithm 1**).

180 The results on the toy Bayesian regression are depicted in **Figure 3**. The approximate posterior means show negligible  
 181 deviations from the analytic posterior means as quantified by very small NRMSEs (as small as 0.002) and very high  $R^2$  (as  
 182 high as 1.0) over all  $n$  sampled during training. This suggests near-perfect estimation of the true posterior means. Further, the  
 183 estimates become increasingly more accurate, as the number of data points  $n$  increases. An inspection of the posterior variances  
 184 over the different  $n$  reveals that the estimated variance follows closely the decrease in analytic variance with increasing  $n$ .  
 185 However, the analytic variance is slightly underestimated at smaller  $n$  and slightly overestimated at larger  $n$ . This pattern is  
 186 also revealed by the KL divergence plot (see **SI**). This result might be attributable to an underexpressive summary network;  
 187 another possibility is that the networks need to be trained longer with smaller learning rate decay.

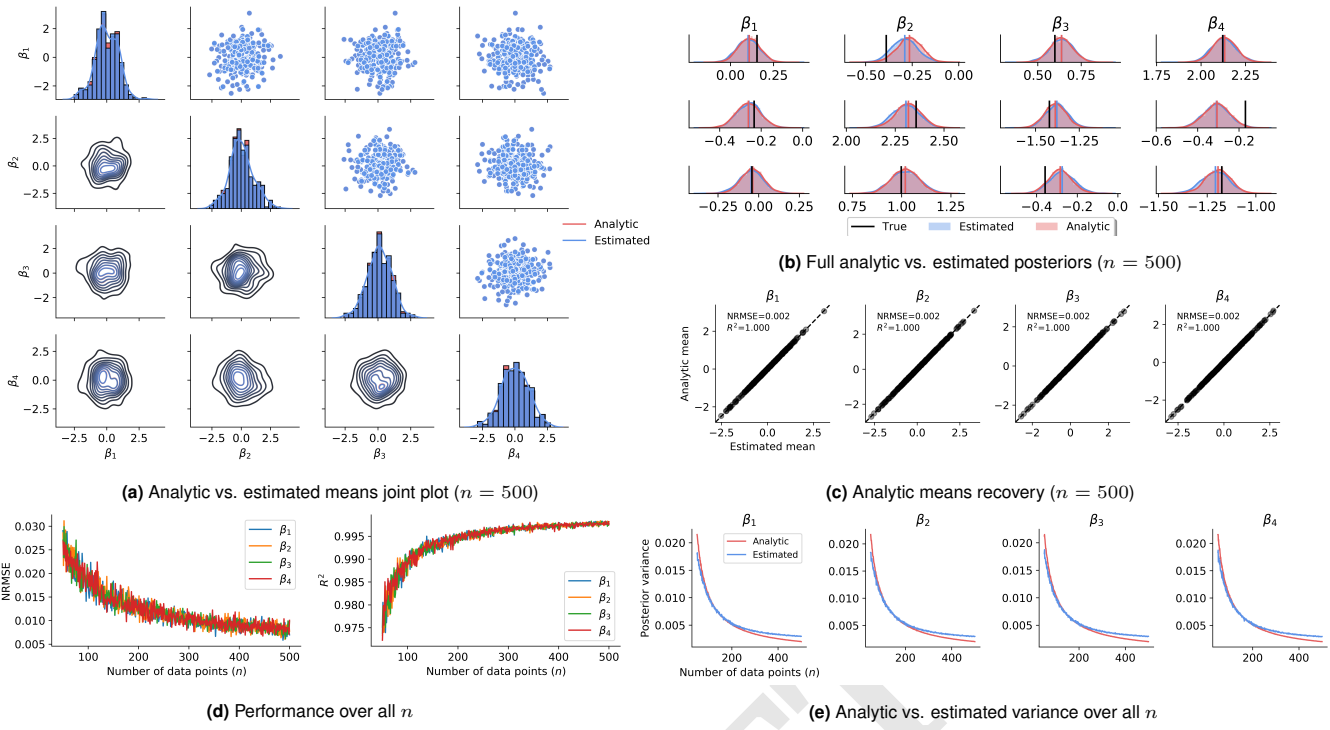


**Fig. 3.** Results on the Bayesian toy regression example. (a) Analytic vs. estimated posterior means on the validation sample. We observe a near-perfect overlap between analytic and estimated posterior means and no spurious covariances; (b) Some example draws from the estimated posteriors. Visual inspections reveals a close match between analytic and estimated posteriors; (c) Posterior mean recovery is almost perfect at  $n = 500$ ; (d) NRMSE and  $R^2$  over all  $n$ . Performance improves with increasing number of data points; (e) Analytic vs. estimated variance over all  $n$ . The analytic variance is slightly underestimated at lower  $n$  and slightly overestimated at higher  $n$ .

**Example 1 - The Ricker Model.** Discrete population dynamics models describe how the number of individuals in a population changes over discrete units of time (7). In particular, the Ricker model describes the number of individuals  $x_{t+1}$  in generation  $t+1$  as a function of the number of individuals in the previous generation  $t$  by the following non-linear equation:

$$x_t \sim \text{Pois}(\rho N_t) \quad [19]$$

$$N_{t+1} = r N_t e^{-N_t + \epsilon_t} \quad [20]$$

for  $t = 1, \dots, T$  where  $N_t$  is the expected number of individuals at time  $t$ ,  $r$  is the growth rate,  $\rho$  is a scaling parameter and  $\epsilon_t \sim \mathcal{N}(0, \sigma^2)$  is random Gaussian noise (17). The Ricker model has no known likelihood function and is thus a suitable candidate for likelihood-free inference. The parameter estimation task is thus to recover  $\theta = (\rho, r, \sigma)$  from the observed one-dimensional time-series data  $\mathbf{x} = (x_1, x_2, \dots, x_T)$  where each  $x_t \in \mathbb{N}$ .

During training of the networks, we simulate time-series from the Ricker model with varying lengths. The number of time points  $T$  is drawn from a uniform distribution  $T \sim \mathcal{U}(100, 500)$  at each training iteration (see the SI for more details about the simulation).

What if the data does not contain information about a given parameter? In this case, any good estimation method should detect this, and return the prior of the particular parameter. To test this, we add a random uniform variable  $u \sim \mathcal{U}(0, 1)$  to the parameter vector  $\theta$  and train the model with this additional dummy variable. Then, we inspect the posterior of  $u$  for uniformity.

The results on the Ricker model are depicted in Figure 3. As evident from the graphics, the parameter recovery becomes better when more time points with data are available (Figure 4c). At  $T = 500$ , the NRMSEs range between 0.015 and 0.063, and the  $R^2$  metrics between 0.997 and 0.952, indicating very good recovery of the posterior means (Figure 4a). The parameter  $\sigma$  seems to be hardest to recover. Inspecting the full posteriors, we further see that the posterior distribution of the dummy noise variable  $u$  closely resembles the prior, as expected due to the complete lack of mutual information between the data  $x$  and  $u$  (Figure 4b). Finally, the plots of the rank statistic computed for SCB suggest no systematic distortions of the posterior across all parameters (Figure 4d). Interpreting deviations from uniformity according to (32), the approximate posteriors of  $r$  and  $\rho$  slightly underestimate the true posterior means, whereas the approximate posterior of  $\sigma$  tends to overestimate the true posterior variance. These deviations appear to be due to the fact that recovery worsens at extreme values of the parameters. This is unsurprising, as the data generated with these parameters is highly implausible, which in some cases might even render a model unidentifiable.

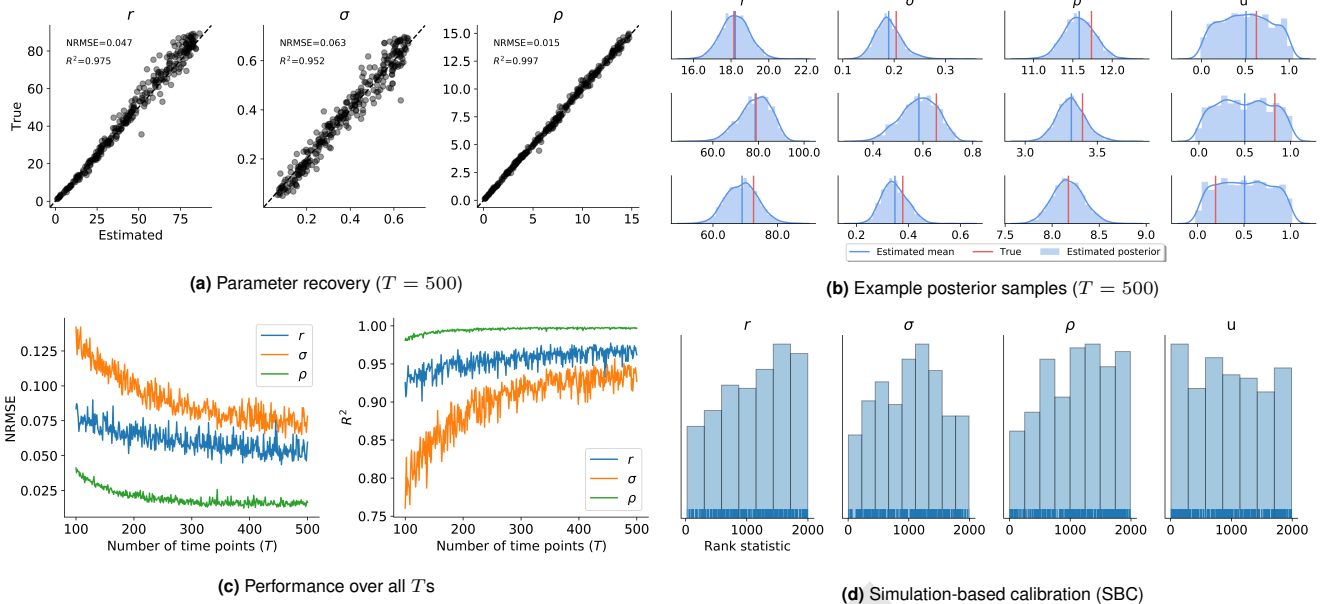


**Fig. 4.** Results on the Ricker model. **(a)** Parameter recovery for the maximum number of generations used during training ( $T = 500$ ); **(b)** Example posteriors for three test datasets. We observe that the posterior of the uniform noise variable  $u$  is equal to the prior, i.e., the method detects that no information is present in data for this variable; **(c)** NRMSE and  $R^2$  performance metrics over all  $T$ 's used in training. We observe that the recovery remains good over all  $T$ 's, and becomes progressively better as more data is available; **(d)** Plots of the rank statistics indicative of the accuracy of the full posterior. Accordingly, the approximate posteriors of  $r$  and  $\rho$  slightly underestimate the true posterior means, whereas the approximate posterior of  $\sigma$  tends to overestimate the true posterior variance.

**Example 2 - The Lévy-Flight Model.** Evidence accumulator models (EAMs) describe (perceptual) decision making by a set of neurocognitively motivated parameters (33). EAMs are most often applied to choice reaction times (RT) data to obtain an estimate of the neurocognitive processes governing observed RT distributions in human and animal participants. Most EAM variants share four underlying assumptions: *i*) information about a stimulus (response option) is accumulated continuously through time; *ii*) stochasticity in the form of noisy accumulation ensures variability; *iii*) empirical response times can be decomposed into a decision time component and a non-decision time component accounting for pre-decisional perceptual (encoding time) and post-decisional motor processes (response execution); and *iv*) a decision is met when the activation of an accumulator exceeds a threshold. In its most general formulation, the forward model of EAMs takes the form of a stochastic differential equation given by (4):

$$dx = vdt + cd\xi \quad [21]$$

where  $dx$  denotes a change in activation of an accumulator,  $v$  denotes the average speed of information processing (often termed the drift rate), and  $d\xi$  represents a stochastic additive component, usually modeled as following a Gaussian distribution centered around 0:  $d\xi \sim \mathcal{N}(0, c^2)$ .

EAMs are particularly amenable for likelihood-free inference, since most members of the family turn out to be intractable (34). This intractability has precluded many interesting applications and empirically driven model refinements. Here, we apply our method to estimate the parameters of the recently proposed Lévy-Flight Model (LFM, (35)). The LFM assumes an *alpha-stable* noise distribution of the evidence accumulation process in order to model "jumps" in the decision process. However, the inclusion of *alpha-stable* noise leads to a model with intractable likelihood; further, to our knowledge, a fully Bayesian treatment of the model is still missing from the literature. The forward equation of the LFM is given by:

$$dx = vdt + \xi dt^{1/\alpha} \quad [22]$$

$$\xi \sim \text{AlphaStable}(\alpha, 0, 1, 0) \quad [23]$$

The LFM has three additional parameters: a threshold  $a$  determining the amount of evidence needed for the termination of a decision process; a relative starting point,  $zr$ , determining the amount of starting evidence available to the accumulator before the actual decision alternatives are presented; and an additive non-decision time  $t_0$ .

During training of the networks, we simulate RT data from two experimental conditions with two different drift rates (see SI for details of the simulation). The parameter estimation task is thus to recover the parameters  $\theta = (v_0, v_1, a, t_0, zr, \alpha)$  from two-dimensional *i.i.d.* RT data  $\mathbf{X} = (\mathbf{x}_1, \mathbf{x}_2, \dots, \mathbf{x}_n)$  containing variable number or RT trials. The number of trials is drawn from a uniform distribution  $n \sim \mathcal{U}(100, 1000)$  at each training iteration.

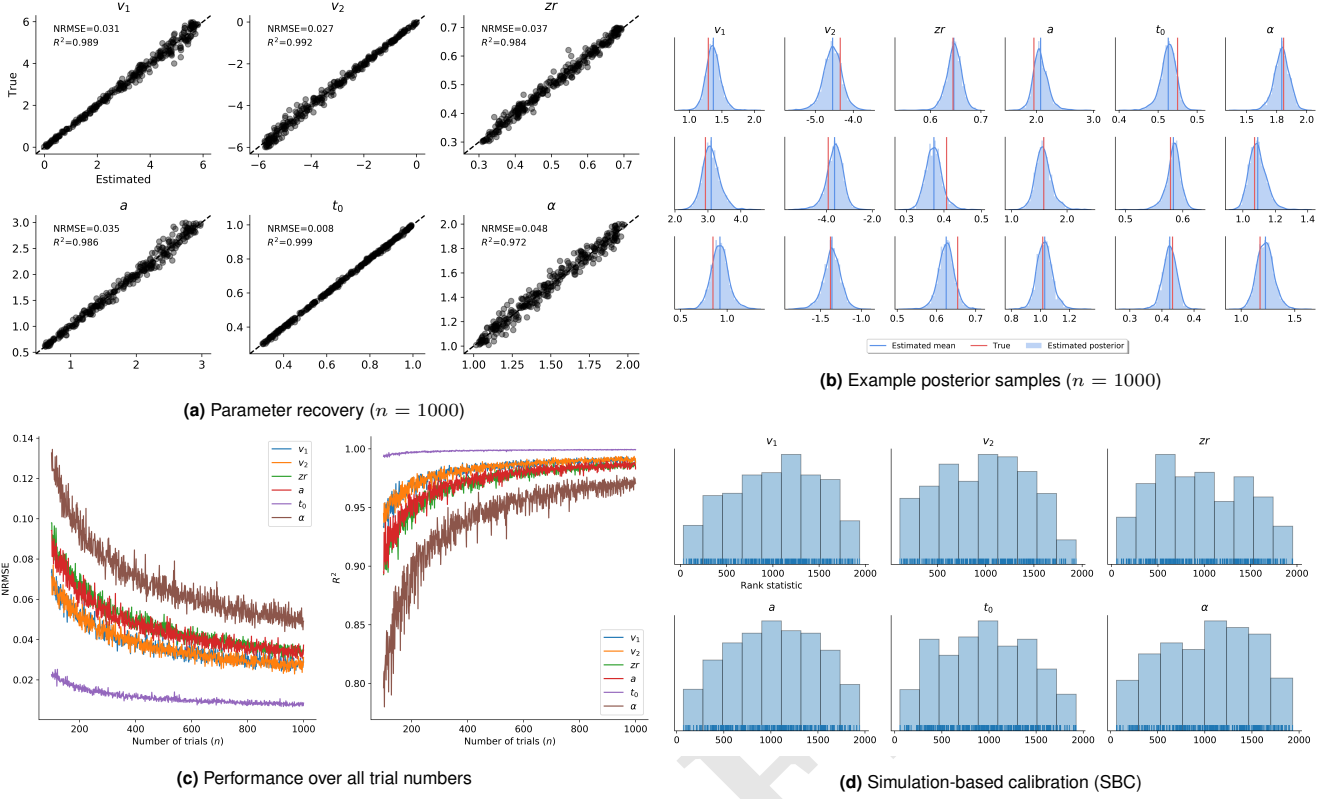


**Fig. 5.** Results on the LFM model. **(a)** Parameter recovery for the maximum number of trials used during training ( $n = 1000$ ); **(b)** Example posteriors for three test datasets; **(c)** NRMSE and  $R^2$  performance metrics over all  $n$  trials used during training. Again, we observe that the recovery remains good overall, and becomes progressively better as more data is available; **(d)** Plots of the rank statistics indicative of the accuracy of the full posterior. Accordingly, the approximate posteriors tend to overestimate the true posterior variance.

220 The results on the LFM model are depicted in Figure 4. XXX

**Example 3 – The Stochastic SIR Model.** Compartmental models in epidemiology are used to describe the stochastic dynamics of infectious diseases as they spread over a population of individuals (8, 9, 36). The parameters of compartmental models encode important characteristics of diseases, such as the rates of infection or recovery from the disease. The stochastic SIR model describes the transition dynamics of  $N$  individuals between three discrete states: susceptible ( $S$ ), infected ( $I$ ), and recovered ( $R$ ). The transition dynamics are given by the following equations:

$$\Delta S = -\Delta N_{SI} \quad [24]$$

$$\Delta I = \Delta N_{SI} - \Delta N_{IR} \quad [25]$$

$$\Delta R = \Delta N_{IR} \quad [26]$$

$$\Delta N_{SI} \sim \text{Binomial}(S, 1 - \exp\left(-\beta \frac{I}{N} \Delta t\right)) \quad [27]$$

$$\Delta N_{IR} \sim \text{Binomial}(I, 1 - \exp(-\gamma \Delta t)) \quad [28]$$

221 where  $S + I + R = N$  give the number of susceptible, infected, and recovered individuals, respectively. The parameter  $\beta$  controls  
222 the transition rate from being susceptible to infected, and  $\gamma$  controls the transition rate from being infected to recovered. The  
223 number of individuals moving from  $S$  to  $I$ , given by  $\Delta N_{SI}$ , and the number of people moving from  $I$  to  $R$ , given by  $\Delta N_{IR}$ ,  
224 over a time interval  $\Delta t$  are modeled as binomial random variables. The above listed stochastic system has no known analytic  
225 solution and thus requires numerical simulation methods for finding optimal parameter values. Cast as a parameter estimation  
226 task, the challenge is to recover  $\theta = \{\beta, \gamma\}$  from three dimensional time-series data  $\mathbf{X} = (\mathbf{x}_1, \mathbf{x}_2, \dots, \mathbf{x}_T)$  where each  $\mathbf{x}_t \in \mathbb{N}^3$  is  
227 a triple containing the number of susceptible ( $S$ ), number of infected ( $I$ ), and recovered ( $R$ ) individuals at time  $t$ .

228 During training of the networks, we simulate time-series from the stochastic SIR model with varying lengths. The number  
229 of time points  $T$  is drawn from a uniform distribution  $T \sim \mathcal{U}(100, 200)$  at each training iteration (see the SI for more details  
230 about the simulation). This range is chosen since we observed that the system reaches an equilibrium in almost all parameter  
231 settings after  $T > 200$ .

232 The results on the SIR model are depicted in Figure XXX.

233 **Example 4 - Single-Cell RNA Sequencing.** Single-cell RNA sequencing (scRNA-seq) is a method to uncover the dynamics of  
234 gene expression within single cells (1, 37). Simulation models for scRNA-seq attempt to mimic the process of sequencing  
235 real data samples by combining statistical and algorithmic procedures. The recently developed *Splat* simulation model (1)  
236 implements a hierarchical model where the mean expression levels for multiple genes are samples from a Gamma distribution,  
237 and the number of times a gene has been sequenced in a cell is then sampled from a Poisson distribution. The output of the  
238 *Splat* simulation is thus a matrix  $\mathbf{X}$  of *Gene x Cell* counts. Figure XXX depicts the *Splat* algorithm for simulating scRNA-seq  
239 data.

240 As a last example for our method, we use simulations from the *Splat* model and attempt to recover the data-generating  
241 parameters. We simulate 250000 *Gene x Cell* count matrices with different parameter settings (see **SI** for details of the  
242 simulation) and discard implausible simulations (e.g., matrices where more than 90% of the counts are 0). We train the  
243 networks for 100 epochs through the entire dataset and evaluate the performance on a separate validation set or matrices.

244 Figure XXX depicts the results...

## 245 Discussion

246 In the current work, we proposed and explored a novel end-to-end likelihood-free method which uses invertible neural networks  
247 to perform approximate Bayesian inference on any mathematical process model. We demonstrated the utility of the method by  
248 applying it to models from various scientific domains exhibiting various data formats and data-generating mechanisms. Further,  
249 we explored two possible training approaches suitable for different simulation scenarios, namely an active learning approach,  
250 and a reference-table approach. Both training approaches lead to excellent recovery of the true parameters throughout the  
251 examples considered in the current work.

252 Our method combines the universal approximation power of deep learning methods with the important uncertainty  
253 quantification assets of Bayesian inference (27, 28). Besides being capable of performing rapid Bayesian inference on intractable  
254 mathematical models, our method provides a general framework for designing reusable “parameter estimation machines” for  
255 various research domains. Moreover, the method is not confined solely to inference on intractable models, but can also prove as  
256 a viable alternative in modeling contexts where standard Bayesian or frequentist inference methods are available, but inference  
257 is nevertheless prohibitively slow.

258 Inspired by previous machine learning approaches to likelihood-free inference (5, 6, 16–20), our method shares many of the  
259 advantages of these methods and further overcomes some important limitations.

260 First, the introduction of separate summary and inference neural network modules renders the invertible inference module  
261 independent of the shape or the size of the observed data. This is achieved by learning a fixed-size vector representation of the  
262 data through the summary module in an automatic, data-driven manner. This is particularly useful in settings where the  
263 most informative summary statistics are not known and thus potential information is lost through the choice of suboptimal  
264 summary function. However, if informative or even *sufficient* statistics are available in a given domain, one might dispose with  
265 the summary module altogether and feed the summary statistics directly to the cINN.

266 Second, we showed that the ML loss optimizes directly the posterior over model parameters of interest, which is in contrast  
267 to ELBO-based methods which optimize a lower-bound on the posterior (20, 30). Thus, inference is exact when the ML  
268 is minimized (22, 24). This *optimal performance* claim is confirmed by our toy Bayesian regression example, in which we  
269 observe negligibly small deviations of the approximate from the true posterior. Further, researchers are often interested in  
270 some summary of the posterior, for instance, the posterior mean or the posterior variance (16, 18). We demonstrated that  
271 our method exhibits excellent recovery of the posterior means throughout the examples. We also showed that the recovery  
272 becomes better with increasing number of observed data points, while the variance of the estimates becomes larger. This is  
273 an important and highly desirable property of any parameter estimation method, as it mirrors the increase in information  
274 following increasing number of data points.

275 Third, the largest computational cost of our method is paid during training. Once trained, the networks can be used and  
276 reused to perform inference on large numbers of datasets within seconds and across a given research domain. Indeed, there are  
277 many instances of research domains where a single model is extensively explored and independently fitted by multiple researches  
278 (CITATION DIFFUSION MODELLING, POPULATION DYNAMICS, NEUROSCIENCE) to test scientific theories about the  
279 modelled process. These research domains are expected to benefit the most from learning the “model universe” once and then  
280 inverting the model multiple times for inference on different datasets. In this regard, our method is similar to the recently  
281 introduced prepaid method (17) which uses a database of pre-computed summary statistics and nearest-neighbors for inference.  
282 Note, however, that our method does not need to store training data on disk, since the “knowledge” about the relationship  
283 between data and parameters is compressed into the networks’ weights. Moreover, all computations involved in our method  
284 benefit from a high degree of parallelism and can thus utilize the advantages of modern graphical processing units (GPUs).

285 These advantages notwithstanding, some limitations of the method deserve a mention. Even though high-level deep learning  
286 libraries, such as *TensorFlow* or *Torch*, allow for rapid and relatively straightforward development of various neural network  
287 architectures, the implementational burden associated with the current method is still reasonably high. In order to ease the  
288 understanding and independent application of the method, we provide fully functioning code to reproduce and study all of the  
289 examples tackled in this paper (<https://github.com/stefanradev93/cINN>). Moreover, we are currently developing a general  
290 user-friendly software, which should abstract away most of the methodological complexities from the user. Another potential  
291 shortcoming of the method is the seemingly overwhelming number of hyperparameters that might require fine-tuning by the user  
292 for optimal performance on a given task. However, we observe that many of the default hyperparameter values are sufficient

293 to achieve excellent performance, and starting with a relatively large default network of 10 ACBs does not appear to hurt  
294 performance or destabilize training, even if the model to be learned is relatively simple. We expect that a single architecture  
295 should be able to perform well on almost all models from a given domain (i.e., a single architecture for decision-making models).  
296 Future research should investigate the question of generality by applying the method to challenging parameter estimation tasks  
297 across different research domains.

## 298 Conclusion

299 As formal theories in various scientific disciplines (especially in the younger sciences, such as, neuroscience, cognitive science,  
300 computational biology, etc.) become increasingly complex, the need for powerful and universally applicable likelihood-free  
301 estimation methods becomes increasingly pressing. In the present work, we addressed this need by introducing a method  
302 potentially applicable to *any* modeling scenario in *any* research domain where simulations from the process model can be  
303 obtained. We hope that the new method will enable researchers from a variety of fields to accelerate model-based inference and  
304 will further prove its utility beyond the examples considered in this paper.

305 **ACKNOWLEDGMENTS.** Please include your acknowledgments here, set in a single paragraph. Please do not include any acknowledgments  
306 in the Supporting Information, or anywhere else in the manuscript.

- 307 1. Zappia L, Phipson B, Oshlack A (2017) Splatter: simulation of single-cell rna sequencing data. *Genome biology* 18(1):174.
- 308 2. Beaumont MA, Zhang W, Balding DJ (2002) Approximate bayesian computation in population genetics. *Genetics* 162(4):2025–2035.
- 309 3. Palestro JJ, Sederberg PB, Osth AF, Van Zandt T, Turner BM (2018) *Likelihood-free methods for cognitive science*. (Springer).
- 310 4. Usher M, McClelland JL (2001) The time course of perceptual choice: the leaky, competing accumulator model. *Psychological review* 108(3):550.
- 311 5. Hwang SJ, Tao Z, Kim WH, Singh V (2018) Conditional recurrent flow: Conditional generation of longitudinal samples with applications to neuroimaging. *arXiv preprint arXiv:1811.09897*.
- 312 6. Lueckmann JM, et al. (2017) Flexible statistical inference for mechanistic models of neural dynamics in *Advances in Neural Information Processing Systems*. pp. 1289–1299.
- 313 7. Wood SN (2010) Statistical inference for noisy nonlinear ecological dynamic systems. *Nature* 466(7310):1102.
- 314 8. Keeling MJ, Rohani P (2011) *Modeling infectious diseases in humans and animals*. (Princeton University Press).
- 315 9. Hethcote HW (2000) The mathematics of infectious diseases. *SIAM review* 42(4):599–653.
- 316 10. Csillery K, Blum MG, Gaggiotti OE, François O (2010) Approximate bayesian computation (abc) in practice. *Trends in ecology & evolution* 25(7):410–418.
- 317 11. Toni T, Stumpf MP (2009) Simulation-based model selection for dynamical systems in systems and population biology. *Bioinformatics* 26(1):104–110.
- 318 12. Turner BM, Sederberg PB (2014) A generalized, likelihood-free method for posterior estimation. *Psychonomic bulletin & review* 21(2):227–250.
- 319 13. Sunnåker M, et al. (2013) Approximate bayesian computation. *PLoS computational biology* 9(1):e1002803.
- 320 14. Mertens UK, Voss A, Radev S (2018) Abrox—a user-friendly python module for approximate bayesian computation with a focus on model comparison. *PLoS one* 13(3):e0193981.
- 321 15. Frazier DT, Martin GM, Robert CP, Rousseau J (2018) Asymptotic properties of approximate bayesian computation. *Biometrika* 105(3):593–607.
- 322 16. Radev ST, Mertens UK, Voss A, Köthe U (2019) Towards end-to-end likelihood-free inference with convolutional neural networks. *British Journal of Mathematical and Statistical Psychology*.
- 323 17. Mestdagh M, Verdonck S, Meers K, Loossens T, Tuerlinckx F (2018) Prepaid parameter estimation without likelihoods. *arXiv preprint arXiv:1812.09799*.
- 324 18. Raynal L, et al. (2018) Abc random forests for bayesian parameter inference. *Bioinformatics* 35(10):1720–1728.
- 325 19. Jiang B, Wu TY, Zheng C, Wong WH (2017) Learning summary statistic for approximate bayesian computation via deep neural network. *Statistica Sinica* pp. 1595–1618.
- 326 20. Papamakarios G, Murray I (2016) Fast  $\epsilon$ -free inference of simulation models with bayesian conditional density estimation in *Advances in Neural Information Processing Systems*. pp. 1028–1036.
- 327 21. Ardizzone L, et al. (2018) Analyzing inverse problems with invertible neural networks. *arXiv preprint arXiv:1808.04730*.
- 328 22. Kingma DP, Dhariwal P (2018) Glow: Generative flow with invertible 1x1 convolutions in *Advances in Neural Information Processing Systems*. pp. 10215–10224.
- 329 23. Grover A, Dhar M, Ermon S (2018) Flow-gan: Combining maximum likelihood and adversarial learning in generative models in *Thirty-Second AAAI Conference on Artificial Intelligence*.
- 330 24. Dinh L, Sohl-Dickstein J, Bengio S (2016) Density estimation using real nvp. *arXiv preprint arXiv:1605.08803*.
- 331 25. Bloem-Reddy B, Teh YW (2019) Probabilistic symmetry and invariant neural networks. *arXiv preprint arXiv:1901.06082*.
- 332 26. Goodfellow I, Bengio Y, Courville A (2016) *Deep learning*. (MIT press).
- 333 27. Kendall A, Gal Y (2017) What uncertainties do we need in bayesian deep learning for computer vision? in *Advances in neural information processing systems*. pp. 5574–5584.
- 334 28. Gelman A, et al. (2013) *Bayesian data analysis*. (Chapman and Hall/CRC).
- 335 29. Abadi M, et al. (2016) Tensorflow: A system for large-scale machine learning in 12th { USENIX } Symposium on Operating Systems Design and Implementation ({ OSDI } 16). pp. 265–283.
- 336 30. Kingma DP, Welling M (2014) Auto-encoding variational bayes. *stat* 1050:1.
- 337 31. Hershey JR, Olsen PA (2007) Approximating the kullback leibler divergence between gaussian mixture models in 2007 IEEE International Conference on Acoustics, Speech and Signal Processing - ICASSP'07. (IEEE), Vol. 4, pp. IV–317.
- 338 32. Talts S, Betancourt M, Simpson D, Vehtari A, Gelman A (2018) Validating bayesian inference algorithms with simulation-based calibration. *arXiv preprint arXiv:1804.06788*.
- 339 33. Ratcliff R, McKoon G (2008) The diffusion decision model: theory and data for two-choice decision tasks. *Neural computation* 20(4):873–922.
- 340 34. Miletic S, Turner BM, Forstmann BU, van Maanen L (2017) Parameter recovery for the leaky competing accumulator model. *Journal of Mathematical Psychology* 76:25–50.
- 341 35. Voss A, Lerche V, Mertens U, Voss J (2019) Sequential sampling models with variable boundaries and non-normal noise: A comparison of six models. *Psychonomic bulletin & review* pp. 1–20.
- 342 36. Sahneh FD, Vajdi A, Shakeri H, Fan F, Scoglio C (2017) Gemfsm: a stochastic simulator for the generalized epidemic modeling framework. *Journal of computational science* 22:36–44.
- 343 37. Ozsolak F, Milos PM (2011) Rna sequencing: advances, challenges and opportunities. *Nature reviews genetics* 12(2):87.